JOURNAL OF THERMOPHYSICS AND HEAT TRANSFER
Vol. 11, No. 1, January–March 1997

Optical Properties of Energetic Materials from Infrared Spectroscopy

R. A. Isbell* and M. Q. Brewster†
University of Illinois at Urbana–Champaign, Urbana, Illinois 61801

A method of determining infrared (2.5–18 μm) optical properties of dielectric, crystalline, particulate solids such as energetic materials was developed based on KBr–FTIR (infrared) spectroscopy. Two techniques (spectral subtraction and baseline shifting) were used to account for light scattering by the KBr matrix. An independent CO_2 laser–spatial filtering measurement was also developed to check the spectral subtraction approach. The method is demonstrated here for the oxidizer ammonium perchlorate (AP). The Rayleigh–Gans limit of light scattering theory was exploited to establish a relationship between the apparent KBr-pellet absorption coefficient and the intrinsic AP absorption coefficient. Dispersion theory was used to determine refractive index from the absorption index for AP. Conventional (nonscattering) FTIR spectroscopy was also used to determine the absorption coefficient for the common solid propellant binder hydroxyl-terminated polybutadiene.

Nomenclature

A = absorbance
d = particle diameter
f_v = particle volume fraction
$I_{t,0}$ = intensity, transmitted and incident, respectively
n = real part of complex refractive index
K_a = absorption coefficient
k = imaginary part of complex refractive index or absorption index
L = pellet thickness
L_{eff} = effective pellet thickness, corrected to account for voids
R_n = normal interface (Fresnel) reflectance
T = sample transmittance
x = particle size parameter
γ = oscillator linewidth
λ_0 = wavelength in vacuum
τ = optical thickness
ω_p = oscillator plasma frequency
ω_0 = oscillator resonant frequency

Introduction

OPTICAL properties of solids are determined by a variety of methods, depending on the properties of the material. For weak to moderately absorbing materials that can be formed into sufficiently thin layers, the absorption coefficient can be determined from transmissivity measurements and application of Beer's law.[1–3] For strongly absorbing materials that can be polished into or deposited onto optically smooth surfaces, reflectance measurements can be analyzed in a variety of ways to yield the optical constants (n and k).[4–8] Many nonmetallic, crystalline materials, however, are not amenable to either of these approaches. Hard, crystalline materials, such as energetic materials (materials used in propellants, explosives, and gas generators capable of isolated, independent combustion), generally have complex infrared spectra with both weakly and strongly absorbing regions; but they are difficult to process into suitably homogeneous and optically smooth samples for either transmission or reflection measurements. In this article a method is discussed for extracting quantitative optical property information for such materials from a well-known technique that has been primarily used for qualitative spectroscopic measurements: KBr–FTIR (infrared) pellet spectroscopy.

In KBr–FTIR pellet spectroscopy, an absorbing powder is uniformly dispersed in infrared transmissive KBr and pressed into pellets for FTIR transmission measurements. This gives data that are quantitative spectrally, but generally only qualitative in terms of the magnitude of the optical properties of the absorbing powder. One factor that makes accurate quantitative measurements of optical properties difficult is that appreciable scattering of radiation occurs at microscopic pores and interfaces in the KBr pellet. This introduces an uncertain contribution into the measured transmissivity and absorbance. Assuming this scattering contribution can be removed, another problem is that the relationship between the apparent absorption coefficient of the pellet and the intrinsic absorption coefficient of the dispersed powder is, in general, unknown.

In this work, a method has been developed that appears promising for solving these problems, making possible the extraction of optical properties from standard, KBr–FTIR transmission measurements. The Rayleigh–Gans limit of scattering by small particles is exploited to establish a connection between the apparent pellet and intrinsic powder absorption properties. Two techniques, called spectral subtraction and baseline shifting, were used to remove the KBr scattering contribution from the measured absorbance. As a check on these scattering correction approaches, a laser (10.6 μm) and spatial filtering technique was developed for making independent absorption measurements. The scattering-corrected, KBr–FTIR data were then used in conjunction with dispersion theory to determine the optical properties of ammonium perchlorate (AP), an important energetic oxidizer used in solid rocket propellants, from 2.5 to 18 μm. Also, conventional FTIR spectroscopy was used to measure the absorption coefficient of hydroxyl-terminated polybutadiene (HTPB) cured with isophorone diisocyanate (IPDI), which is an important binder in AP-composite propellants.

Received June 21, 1996; revision received Sept. 6, 1996; accepted for publication Sept. 10, 1996.

*Graduate Research Assistant, Department of Mechanical and Industrial Engineering, 1206 West Green Street.

†Professor of Mechanical Engineering, Department of Mechanical and Industrial Engineering, 1206 West Green Street. Associate Fellow AIAA.

Theoretical Considerations

The transmissivity of a homogeneous (nonscattering) plane layer in air subject to normal incident monochromatic radiation is given by[9]

$$T = \frac{I_t}{I_0} = \frac{(1 - R_n)^2 e^{-\tau}}{1 - R_n^2 e^{-2\tau}} \tag{1}$$

where $\tau = K_a L$ is the optical thickness. This accounts for multiple reflection of radiation between the two interface boundaries, where R_n, the normal Fresnel interface reflectance, is given by

$$R_n = \frac{(n - 1)^2 + k^2}{(n + 1)^2 + k^2} \tag{2}$$

The absorption coefficient and absorption index k of a homogeneous material are related by

$$K_a = 4\pi k/\lambda_0 \tag{3}$$

where λ_0 is the vacuum (~air) wavelength of the incident intensity. If the layer consists of a nonabsorbing, nonscattering matrix (say, KBr without voids) and an absorbing sample material of the same refractive index, extinction of incident radiation by scattering will be negligible. Furthermore, if the particle size d of the absorbing component is small such that $K_a d << 1$, then the effective absorption coefficient of the layer is the intrinsic absorption coefficient of the absorbing constituent weighted by its volume fraction $K_a f_v$. In particle light scattering theory this approximation is known as Rayleigh–Gans scattering,[9] and carries with it the formal restrictions $2x|\tilde{n} - 1| << 1$ and $|\tilde{n} - 1| << 1$, where $x = \pi d/\lambda$, $\lambda = \lambda_0/n$, and $\tilde{n} = n - ik$. If the condition $K_a d << 1$ is not satisfied, a more complicated particle light scattering theory might be used to relate the pellet volumetric optical properties to those of the absorbing constituent particles; however, particle geometry (shape and size) would become important and the technique would lose its advantage of accuracy. If the condition $K_a d << 1$ is not satisfied, but the data are analyzed assuming that the pellet absorption coefficient is $K_a f_v$ anyway, K_a will be underpredicted.

In KBr pressed pellets there are discontinuities in refractive index at the boundaries between KBr particles and between KBr and sample particles (the latter contribution, scattering by sample particles, is usually negligible because their concentration is so low, $f_v << 1$), which cause scattering of radiation. Scattering can be accounted for by including a scattering coefficient K_s, which is additive with the absorption coefficient. Thus, the optical thickness of the layer is based on the extinction coefficient that is the sum of the scattering and absorption coefficients:

$$\tau = K_e L, \qquad K_e = K_a f_v + K_s \tag{4}$$

To account for the (typically very small) volume fraction in the pellets occupied by voids caused by imperfect packing, the actual sample thickness L was reduced slightly, $L_{\text{eff}} = L(\rho_{\text{act}}/\rho_{\text{theo}})$, where ρ_{act} is actual pellet density, and ρ_{theo} is theoretical pellet density (no voids). The sample f_v now becomes the (more easily measured) value based on the assumption of no voids (i.e., volume fraction of sample particles relative to KBr and sample only). Equation (4) thus becomes

$$\tau = K_e L_{\text{eff}}, \qquad K_e = K_a f_v + K_s \tag{5}$$

Substituting Eq. (5) into Eq. (1) and rearranging gives

$$A = \log(1/T) = \log[(1 - R_n)^{-2}] + 0.4343 L_{\text{eff}}(K_a f_v + K_s) + \log(1 - R_n^2 e^{-2\tau}) \tag{6}$$

Equation (6) is the appropriate relation to apply in the Rayleigh–Gans limit to uncorrected (for scattering and reflection) KBr pellet transmission data if quantitative absorption information is desired. One difficulty in doing so, particularly in the near infrared and shorter wavelength regions, is the fact that the scattering coefficient can be of nonnegligible magnitude compared with the volume fraction weighted absorption coefficient, making an independent measurement of the scattering coefficient or an equivalent scattering correction necessary. In the KBr–FTIR pellet technique the scattering contribution was removed from the transmission measurement data by two techniques: 1) spectral subtraction and 2) baseline shifting. The spectral subtraction correction is discussed in the next paragraph. In baseline shifting, the background or baseline of the FTIR transmission spectrum (which is a result of scattering and reflection losses) is curve-fit and subtracted from the spectrum. This effectively removes the scattering and reflection contributions. To account for this in the absorbance data reduction equation [Eq. (6)], the values of K_s and R_n should be set to zero, giving

$$A = \log(1/T) = 0.4343 K_a f_v L_{\text{eff}} \tag{7}$$

This is the form of Beer's law appropriate for analyzing KBr–FTIR transmission data when scattering and reflection losses have been accounted for, such as with baseline shifting (and as discussed later with spectral subtraction). Equation (7) indicates a linear relationship between absorbance and the product $f_v L_{\text{eff}}$ with the slope of A vs $f_v L_{\text{eff}}$, giving the absorption coefficient. Both f_v and L_{eff} were varied independently in this investigation. Linear regression was applied to absorbance data on a spectral basis and absorption coefficients were extracted from the slopes.

To check the baseline shifting correction, another scattering correction approach was used, called spectral subtraction. In spectral subtraction, pure KBr pellets were prepared that had as nearly as possible the same scattering coefficient as similar KBr/AP pellets, but without AP (see the Sample Preparation section and Ref. 10). The pure KBr pellets were used for reference measurements to quantify and compensate for the KBr scattering contribution. Transmissivity was measured on both absorbing (KBr/AP) and nonabsorbing (KBr) pellets for various optical thicknesses (varying thickness and AP volume fraction). The ratio of the transmitted signal for KBr/AP (scattering/reflection plus absorption losses) to that for pure KBr (scattering/reflection losses only) can be taken as the scattering-corrected (and to at least a partial degree reflection-corrected) transmissivity T for the absorbing pellet. The resulting transmissivity and absorbance are

$$A = \log(1/T) = 0.4343 K_a f_v L_{\text{eff}} - \log[1 - R_n^2 \exp(-2K_s L_{\text{eff}})] + \log[1 - R_n^2 \exp[-2(K_a f_v + K_s)L_{\text{eff}}]] \tag{8}$$

Equation (8) comes from applying Eq. (6) twice, once with and once without absorbing AP present, and taking the ratio of the transmissivities or the difference of the absorbances. To a good approximation the last two terms in Eq. (8) were negligible for all of the pellet thicknesses used in this study, giving again Eq. (7). Equation (7) is therefore appropriate for data obtained using spectral subtraction as well as baseline shifting.

The use of spectral subtraction with the KBr–FTIR method is based on the assumption of negligible forward scattering contribution being measured in the transmitted signal. To check this assumption another independent measurement using spectral subtraction was developed called laser and spatial filtering. In the laser and spatial filtering technique, a CO_2 laser beam (10.6 μm) was passed through a KBr pellet and focused on a pinhole aperture. Radiation scattered by the pellet was defocused in an annulus about the beam axis and blocked by the pinhole while unscattered, transmitted energy was passed

to a detector. Transmissivity was measured on both pure KBr and KBr/AP pellets of varying optical thickness as described previously for spectral subtraction. Equations (6) and (7) were used to analyze the data. These measurements served as a check on the FTIR measurements (both baseline shifting and spectral subtraction) at 10.6 μm.

The measured spectra for absorption index k, as determined by the FTIR–spectrometry technique, were curve-fitted using an optimization routine and dispersion theory relations[9]:

$$n^2 - k^2 = n_e^2 + \sum_j \frac{\omega_{p,j}^2(\omega_{0,j}^2 - \omega^2)}{(\omega_{0,j}^2 - \omega^2)^2 + \gamma_j^2\omega^2} \tag{9}$$

$$2nk = \sum_j \frac{\omega_{p,j}^2\gamma_j\omega}{(\omega_{0,j}^2 - \omega^2)^2 + \gamma_j^2\omega^2} \tag{10}$$

The residual value of refractive index n_e occurs at the short wavelength end of the spectral interval of interest, which is the visible/near infrared region in this case. Its value results from electronic transitions in the ultraviolet region. This procedure resulted in values for the oscillator parameters (ω_p, ω_0, and γ) and n.

The analysis through Eq. (10) is based on the assumption of theoretically perfect spectral resolution or spectral purity, which is a reasonable representation for most of the FTIR measurements reported here. In practice, however, CO_2 lasers can emit radiation at multiple spectral lines simultaneously. Thus, the measured CO_2 laser transmissivity can be affected by radiation at various wavelengths and polychromatic irradiation effects need to be considered for the laser–spatial filtering technique. This can be done by applying Eq. (7) on a spectral basis, integrating over the wavelength range of the incident radiation, and defining an effective total absorption coefficient to give the following equations:

$$T_{\text{tot}} = \frac{I_{t,\text{tot}}}{I_{0,\text{tot}}} = \exp(-K_{a,\text{tot}} f_v L_{\text{eff}}) \tag{11}$$

$$K_{a,\text{tot}} = \left(\frac{-1}{f_v L_{\text{eff}}}\right) \ell n \left[\frac{\int_{\lambda_1}^{\lambda_2} I_{0,\lambda} \exp(-K_{a,\lambda} f_v L_{\text{eff}})\, d\lambda}{\int_{\lambda_1}^{\lambda_2} I_{0,\lambda}\, d\lambda} \right] \tag{12}$$

According to Eq. (12), for the same spectral incident intensity, wavelengths of weaker absorption will be weighted more heavily in determining the total, effective absorption coefficient using total transmissivity measurements. Thus, a knowledge of the spectral content of the incident radiation is important in interpreting total transmissivity data.

Experimental Methods

KBr–FTIR Technique

The spectrometer used in these measurements was a Nicolet Magna-IR 750 with an infrared source, KBr beamsplitter, and a deuterated triglycine sulfate (DTGS) detector. Mirror displacement alignment was verified by matching the peaks of a sample polystyrene spectrum with those of a known reference spectrum. Spectra were averaged over 64 scans with a mirror velocity of 0.6329 mm/s, sampled at 2 cm^{-1} resolution, and processed with Happ–Genzel apodization with no zero filling. Beamsplitter efficiency and detector response established a practical spectral range of 4000–400 cm^{-1} (2.5–25 μm). The interferograms were digitized with 16,672 scan points and fast Fourier transformed over 16,384 points centered at the peak interferogram position, leading to 3736 spectral points at 0.9643 cm^{-1} intervals over 4000.8486–399.2170 cm^{-1}. The sample compartment was purged with nitrogen gas to reduce the effects of CO_2 and water vapor absorption lines. A small source drift of 0.03% was typically present in transmittance spectra with noise levels up to 0.20% in the participating spectral regions of water vapor. Noise levels peaked at 1% in the low wave number end of the spectrum because of beamsplitter efficiency and detector response.

Laser–Spatial Filtering Technique

In the laser and spatial filtering transmissivity measurements, a 50-W CO_2 laser was detuned to a power of 4 W and the 6.3-mm-diam ($1/e^2$ power point) beam was passed through a sample compartment and focused by a 100-mm focal length lens to a 200 μm high-power pinhole aperture. The pinhole blocked the scattering annulus and passed a diverging conic wave front to a photoelectromagnetic (PEM) detector. The rms signal was monitored by a digital multimeter. Fine positioning of the sample, lens, and pinhole aperture was accomplished by a variety of tilt and translation stages. The detector was positioned along the wave front axis so that a maximum signal was obtained. Sample transmission was measured by taking the ratio of the signals with and without a sample in place.

Sample Preparation

AP and KBr powder were baked separately overnight in a vacuum oven at 150°C and 25-mm-Hg vacuum. The powder was then hand ground with an agate mortar and pestel for 15 min until most of the particles were submicron in size. Small amounts of each material were weighed to within 0.0001 g and mixed to obtain the desired concentrations. The powder was placed in a hardened stainless-steel vial and ball assembly and mixed for 1 min in an amalgamator. The mixtures were pressed into pellets at 170 MPa (25 kpsi) for 5 min in an evacuable 13-mm die. Spectral subtraction samples were crushed, ground, and pressed again, resulting in a slightly higher scattering coefficient (a few percent) compared to nonreprocessed samples. However, the scattering coefficient was more consistent for the reprocessed samples, which is an important characteristic for doing spectral subtraction.

The binder was a mixture of 84% mass fraction HTPB, 6% IPDI, and 10% dioctyl acetate (DOA). The liquid constituents were weighed to within 0.0001 g and stirred in a glass jar with an electric mixer for 30 min to ensure uniformity. This process introduced tiny air pockets into the uncured binder that were removed by subjecting the mixture to a vacuum in an oven at 60°C for 3 h. Various film thicknesses were obtained by curing the mixture between Plexiglas® strips at 60°C and atmospheric pressure for 72 h. The samples were removed from the strips and placed in sample holders for mounting in the spectrometer sample compartment. Film thicknesses were measured to within 0.01 mm and varied over 0.02–0.15 mm.

Results

FTIR Results

Figure 1 shows typical transmittance and absorbance spectra for AP/KBr and HTPB/IPDI binder. The absorbance baseline for AP/KBr shows a gradual decrease with increasing wavelength. This is because of a reduction in the scattering coefficient of the KBr pellets with increasing wavelength as predicted by light scattering theory. This effect was stronger in thicker pellets relative to thinner ones as a result of a larger value of $K_{s,\text{KBr}}L_{\text{eff}}$ at any given wavelength. Absorbance baselines for the binder were relatively flat, regardless of sample thickness, indicating negligible scattering in binder samples.

The variation in measured absorbance with increasing pellet thickness at 10.60358 μm is shown in Fig. 2 (this wavelength was the closest to 10.600 μm that was sampled). Figure 2a shows absorbance vs L_{eff} for KBr/AP pellets, which were specially prepared for spectral subtraction, that is, with similar scattering coefficients. Three different AP volume fractions are shown ($f_{v,\text{AP}} = 0$, 0.00704, and 0.00996). Linear regression was

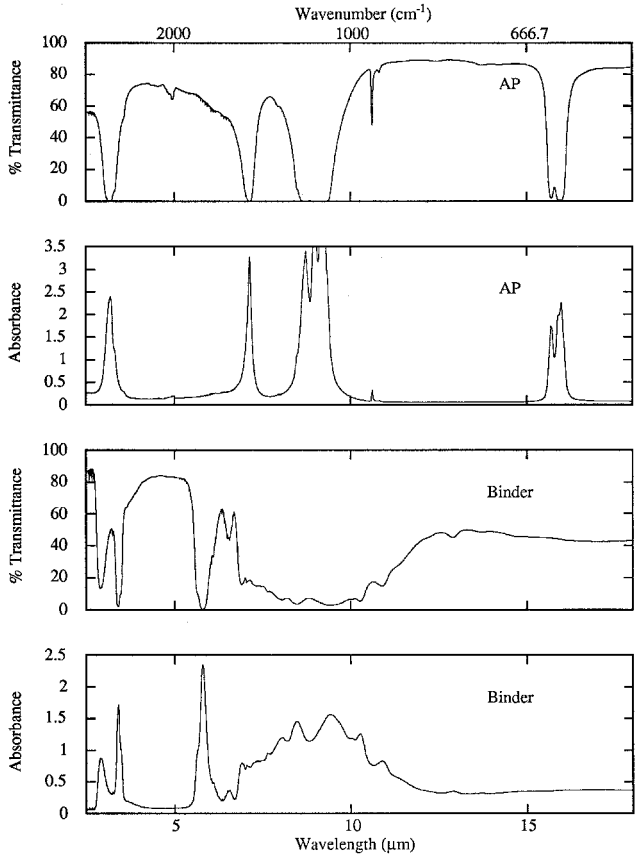

Fig. 1 Typical transmittance and absorbance spectra for AP/KBr and HTPB binder.

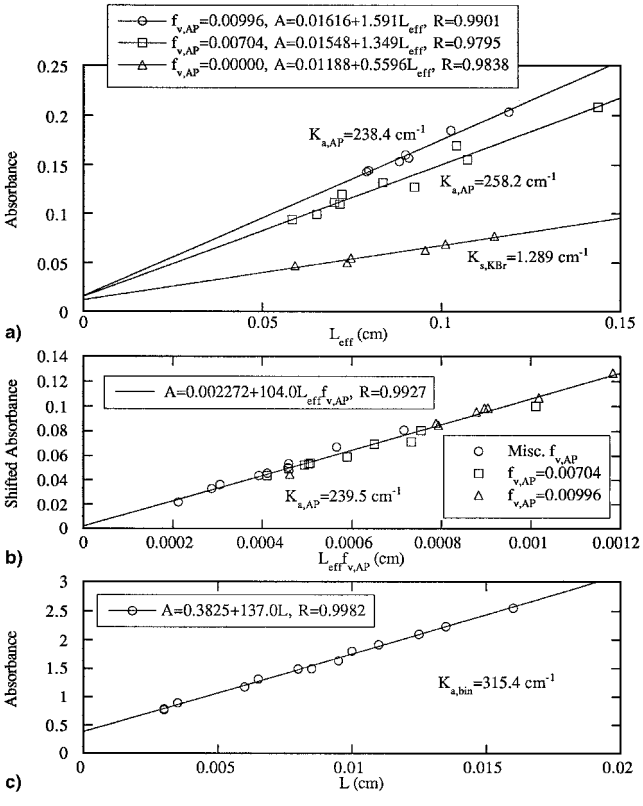

Fig. 2 Absorbance for a) spectral subtraction analysis of AP/KBr samples, b) baseline shifting analysis of AP/KBr samples, and c) HTPB binder (all at 10.60358 μm). Straight lines are curve fits for *A*; *R* is the correlation coefficient.

performed for each value of $f_{v,AP}$. The regression parameters are shown in Fig. 2a. The parameters for the pure KBr pellets ($f_{v,AP} = 0$) were used in Eq. (6) to determine the scattering coefficient, $K_{s,KBr} = 1.3\ cm^{-1}$. Using this scattering coefficient and the regression parameters for the other two cases (including AP), the absorption coefficient of AP was obtained using Eq. (6) as 258 and 238 cm^{-1} for the $f_{v,AP} = 0.00704$ and 0.00996 cases, respectively. The absorbance intercepts ($L_{eff} = 0$ in Fig. 2a) correspond to normal reflectance values of approximately 0.02. This is about what would be expected for KBr, which has a refractive index of $n = 1.525$ at 10.6 μm (ignoring interference effects the normal reflectance would be 0.04).

Figure 2b shows the absorbance for KBr/AP pellets as obtained using baseline shifting. Since consistency of scattering properties is not so important for baseline shifting, additional samples were prepared and used in addition to the specially prepared spectral subtraction samples. A linear regression was performed and the fitting parameters are shown in Fig. 2b. The correlation was very good (as indicated by the correlation coefficient $R = 0.9927$) and the slope gave an AP absorption coefficient of 239 cm^{-1}. The intercept was nearly zero as it should be since account has been made for reflection.

Figure 2c shows the absorbance for the binder samples. A Beer's law analysis of this data neglecting scattering [Eq. (1)] results in an intercept of 0.383 absorbance units and an absorption coefficient of 315 cm^{-1}. This intercept corresponds to a surface reflectance of 35%, which seems unrealistically high. The problem has to do with the assumption of constant absorption coefficient in Beer's law and the effect of polymer chain alignment on K_a. As the binder layer thickness decreases, the degree of polymer chain alignment (parallel to the layer) increases. Therefore, the absorption coefficient becomes more anisotropic for thinner samples. For incident radiation propagating perpendicular to the polymer chains, the absorption coefficient apparently increases with decreasing sample thickness. This results in a lower apparent absorption coefficient

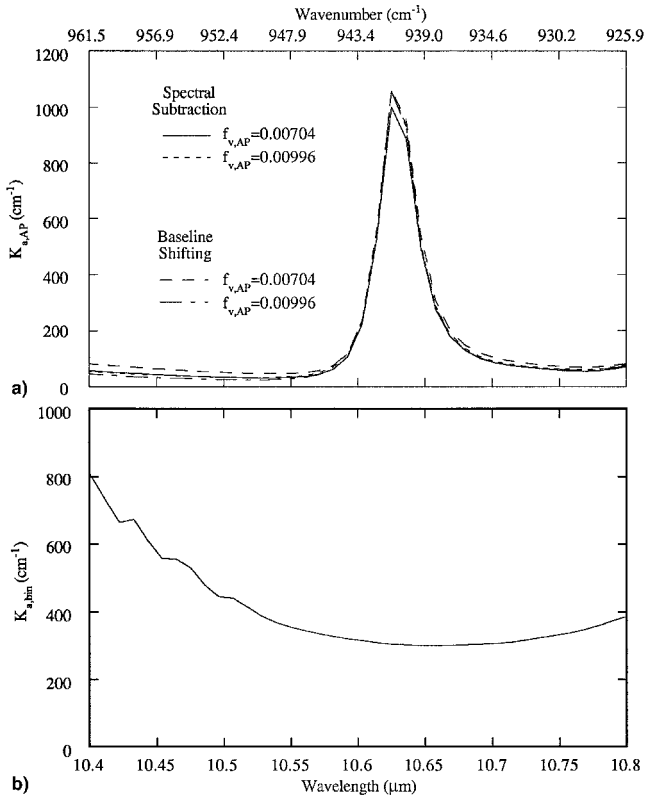

Fig. 3 Absorption coefficient for a) AP and b) HTPB binder near 10.6 μm.

and a higher apparent interface reflectance when the absorbance data are analyzed using Beer's law, assuming constant absorption coefficient. In an effort to correct for this systematic error, near-normal (28 deg) specular reflectance was measured on 1-cm-thick binder samples. The resulting reflectance was 7.2%, which confirms that the absorbance intercept in Fig. 2c overpredicts by a factor of 5 the actual interface reflectance and that the binder absorption coefficient so derived is probably a function of sample thickness. To obtain a better estimate of the bulk absorption coefficient of binder with random polymer chain orientation, another linear fit of absorbance data was done using only the data for the thickest binder samples and forcing the curve through the absorbance intercept corresponding to the measured reflectance. The resulting slope gave a bulk absorption coefficient of $K_{a,\mathrm{bin}} = 361\ \mathrm{cm}^{-1}$. The corresponding absorption index from Eq. (3) is $k_{\mathrm{bin}} = 0.030$ and the refractive index from Eq. (2) is $n_{\mathrm{bin}} = 1.73$.

Using the methods described earlier for 10.60358-μm wavelength, absorption coefficients were calculated at each sampled wavelength. Figure 3a shows the $K_{a,\mathrm{AP}}$ spectra near 10.6 μm determined by each method for the AP/KBr sample groups. Polynomial fits were made of the data nearest 10.600 μm to yield $K_{a,\mathrm{AP}}$ values that ranged from 185 to 211 cm^{-1}, depending on the method. Spectral subtraction and baseline shifting yielded similar results throughout the measured spectral range. A composite baseline shifting analysis of all the samples (similar to that done in Fig. 2b) gives $K_{a,\mathrm{AP}} = 191\ \mathrm{cm}^{-1}$ at 10.600 μm. Comparing this value with that at 10.60358 μm, 239 cm^{-1}, shows how rapidly $K_{a,\mathrm{AP}}$ varies in this region. This rapid variation is because of a relatively weak resonance at 10.63 μm, which corresponds to the perchlorate ion breathing frequency.[11] Figure 3b shows that the absorption coefficient for the binder is much more constant near 10.6 μm than that for AP.

Figure 4 shows absorption spectra over the range 2.5–18 μm. Some of the peaks are truncated because of insufficient transmission at these wavelengths. AP has a relatively simple

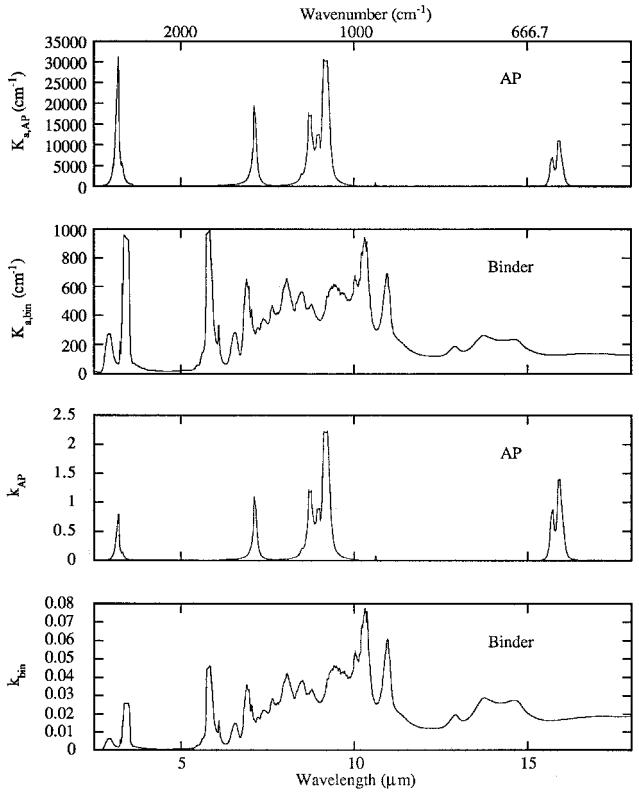

Fig. 4 Absorption coefficient and index for AP and HTPB binder over 2.5–18 μm.

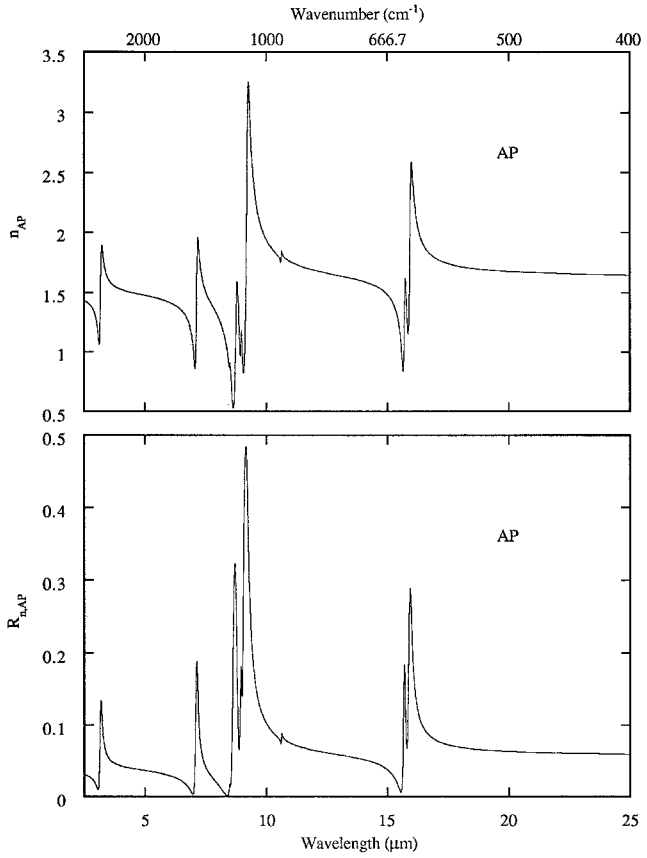

Fig. 5 Refractive index and normal reflectance for AP from dispersion theory.

structure with strong ionic bonds as indicated by few, widely spaced, strong bands. The binder is a polymeric mixture of materials with a more complex molecular structure characterized by prevalent covalent bonding. Detailed discussions of molecular structure and bond–peak assignments are available for AP[8,11–14] and HTPB.[15–17]

Figure 5 shows the refractive index spectrum for AP as obtained from dispersion theory and curve fitting of the absorption spectrum. The visible region refractive index was taken as $n_{e,\mathrm{AP}} = 1.484$. Nine Lorentzian oscillators were assumed[9] and the oscillator parameters are given in Table 1. The normal reflectance spectrum $R_{n,\mathrm{AP}}$ as determined from Eq. (2) is also shown in Fig. 5.

Laser and Spatial Filtering Results

With the laser and spatial filtering method, transmissivity measurements were made for two groups of samples: group 1 with AP volume fractions of 0.0000, 0.01769, 0.02307, and 0.03585; and group 2 with AP volume fractions of 0.0000, 0.00704, and 0.00996, as shown in Fig. 6. The scattering coefficient [from Eq. (6) for $f_{v,\mathrm{AP}} = 0$] for group 1 (1.2 cm^{-1}) appeared to be slightly higher than for group 2 (0.8 cm^{-1}). The absorbance intercepts for the two groups (0.033 and 0.042) were reasonably close to the expected value (0.035) corresponding to a normal reflectance of 0.04. As expected, transmissivity decreases as AP volume fraction increases for a given thickness. Linear regression fits were made for each absorbance data set, forcing the curve through the pure KBr intercept for each group, respectively. Absorption coefficients were extracted for each data set (after correction for scattering) from the various slopes using Eq. (6). The resulting values of $K_{a,\mathrm{AP}}$ ranged from 239 to 276 cm^{-1}, as shown in Fig. 6.

Figure 7 shows the corrected (spectral subtraction) absorbance obtained when the results of Fig. 6 are modified by subtracting the reflectance and scattering contributions as in-

Table 1 Oscillator parameters for AP

Oscillator	ω_o, s^{-1}	γ, s^{-1}	ω_p, s^{-1}
1	$5.890(10^{14})$	$1.785(10^{13})$	$1.634(10^{14})$
2	$2.628(10^{14})$	$3.569(10^{12})$	$5.636(10^{13})$
3	$2.213(10^{14})$	$1.315(10^{12})$	$7.515(10^{12})$
4	$2.142(10^{14})$	$2.818(10^{12})$	$4.415(10^{13})$
5	$2.095(10^{14})$	$1.691(10^{12})$	$2.067(10^{13})$
6	$2.036(10^{14})$	$2.912(10^{12})$	$8.642(10^{13})$
7	$1.768(10^{14})$	$5.636(10^{11})$	$6.200(10^{12})$
8	$1.195(10^{14})$	$6.387(10^{11})$	$1.371(10^{13})$
9	$1.177(10^{14})$	$9.393(10^{11})$	$2.630(10^{13})$

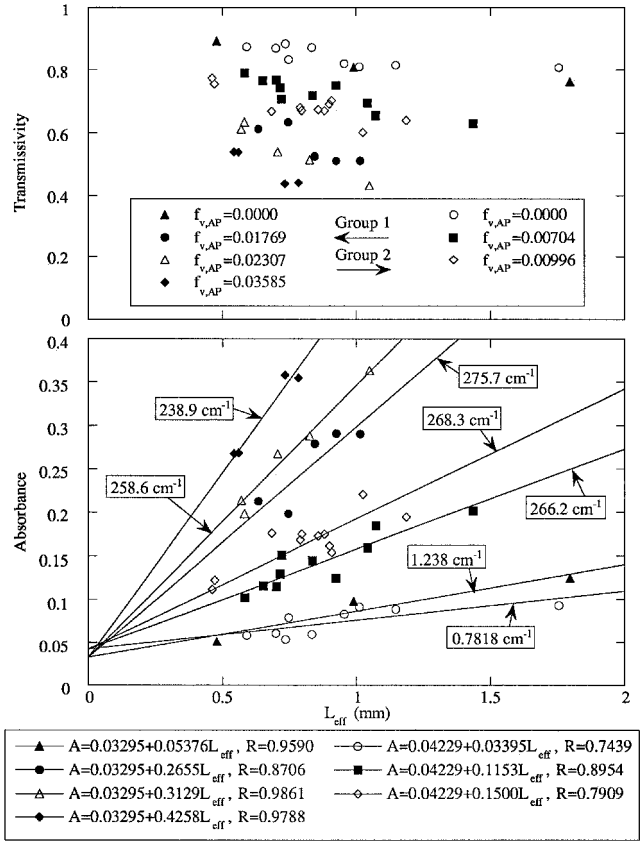

Fig. 6 Transmissivity and absorbance for AP laser and spatial filtering samples (10.60 μm). Straight lines are curve fits for A; R is the correlation coefficient. Values in cm^{-1} are K_a (>200) and K_s (<2).

terpolated from the regression fits for each respective data set and combined. A linear fit of the corrected absorbance data of Fig. 7 gives $K_{a,AP} = 239$ cm^{-1}. This value agrees well with the results obtained from the FTIR measurement (recall that at 10.60358 μm the FTIR technique also gave 239 cm^{-1}). This agreement seems particularly significant considering that in this wavelength region the absorption coefficient varies rapidly because of the perchlorate ion band at 10.63 μm. The fact that the linear fit does not quite pass through the origin as it should according to Eq. (7) is partly because of the fact that Eq. (7) is an approximation. For the property values applicable to AP/KBr pellets ($K_a f_v \approx 2$ cm^{-1}, $K_s \approx 1$ cm^{-1}, and $R_n \approx 0.04$) the more rigorous Eq. (8) exhibits a weak curvature for $f_v L_{eff}$ values less than about 0.02 mm and is very nearly linear for larger $f_v L_{eff}$ values. Linear extrapolation from the linear region of Eq. (8) (large $f_v L_{eff}$ values) to the region of $f_v L_{eff}$ approaching zero results in a zero intercept of $A \sim 0.0015$, which is not enough to account for the observed linear fit intercept of $A \sim 0.01$. The additional contribution to the zero intercept value of A could be because of the lack of spectral purity in the laser beam. Equation (8) is based on the assumption of perfect

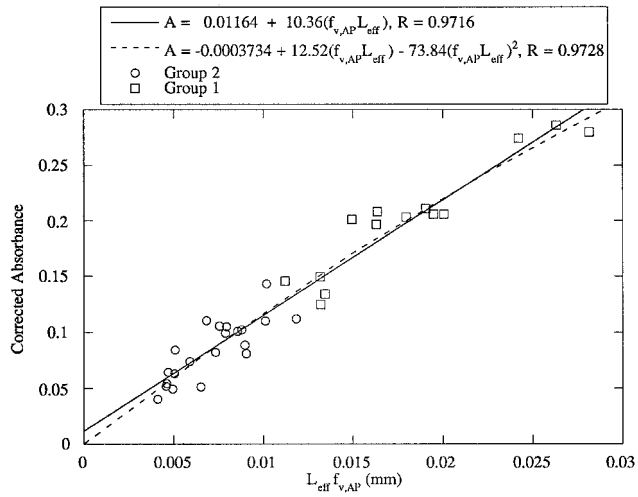

Fig. 7 Composite absorbance for AP laser and spatial filtering samples (10.60 μm). Straight lines are curve fits for A; R is correlation coefficient.

monochromaticity of the radiation. The effect of multiple lasing lines would be additional deviation from linearity of the measured corrected absorbance as a function of $f_v L_{eff}$. To illustrate this effect, a second-order polynomial was also fit through the data of Fig. 7. This resulted in a near-zero intercept and a curvature typical of that predicted by Eqs. (11) and (12) when multiple lines are assumed. In the optically thin limit ($L_{eff} f_{v,AP} \to 0$), the second-order fit results in $K_{a,tot} = 288$ cm^{-1} and corresponds to an absorption coefficient-weighted average of spectral incident intensity. At $L_{eff} f_{v,AP} = 25$ μm, the second-order fit results in $K_{a,tot} = 203$ cm^{-1}. This variation (288–203 cm^{-1}) probably represents the effect of the variation of K_a with wavelength for AP near 10.6 μm, combined with multiple line laser output. Because it was not possible to perform an independent measurement of the laser spectral purity, it is difficult to draw firm conclusions from these results. Still, the laser spatial filtering results can be usefully viewed two ways. Assuming the laser output was near 10.60 μm, the agreement can be seen as supporting the assumption that forward scattering in the KBr–FTIR measurements was indeed negligible and that spectral subtraction was justified with the FTIR data. Or, assuming that the FTIR forward scattering was negligible, the results could be viewed as supporting the conclusion that the laser had a reasonably spectrally pure output near 10.60 μm with some spectral nonpurity as evidenced by curve fits of Fig. 7. In either case, the laser spectral filtering results serve as useful verification of the KBr–FTIR pellet method in general, and the baseline shifting scattering correction method in particular. Table 2 is a summary of optical properties determined at 10.6 μm for AP and HTPB binder.

Discussion

Both the FTIR and laser-spatial filtering techniques used in this study are dependent on the assumption of Rayleigh-Gans scattering to obtain accurate absorption coefficient data for crystalline materials. If the conditions for Rayleigh–Gans scattering are not satisfied, but the data are analyzed under that assumption, the absorption coefficient K_a will be underpredicted. The key condition that must be satisfied is that the particles be optically thin $K_a d << 1$. In this study, particles were ground to the submicron size range, as verified by optical microscopy, but no attempt at a more accurate size determination was made. Assuming an effective average absorbing particle size of 0.5 μm and using 0.3 as the maximum limit of $K_a d$ gives a maximum absorption coefficient of 6000 cm^{-1}. Thus, there is high confidence in the accuracy of the indicated absorption coefficients below this value and an increasing (although as yet unquantified) tendency for underestimation in

Table 2 Optical properties for AP and HTPB binder at 10.600 μm

Material	K_a, cm^{-1}	k	n	R_n, %
AP	191 ± 15 (239)[a]	0.016 (0.020)[a]	1.75	7.46
Binder[b]	361 ± 15	0.030	1.73	7.18

[a]At 10.60358 μm.
[b]Based on reflectance measurements and corrected for polymer chain alignment.

the values reported above 6000 cm^{-1}. For AP, the indicated absorption coefficient exceeded 6000 cm^{-1} in the strongest absorption bands, and therefore, further measurements should be conducted to better quantify the potential error in the AP measurements in the band regions. Near 10.6 μm, however, where the laser–spatial filtering technique was used with AP to confirm the FTIR measurements, the absorption coefficient of AP (near 200 cm^{-1}) was well below the 6000 cm^{-1} threshold value. Even at 10.6-μm, error estimation with either technique is difficult (as discussed in the Laser and Spatial Filtering Results section), with the FTIR technique because of unknown uncertainty associated with background subtraction, and with the laser-spatial filtering technique because of unknown uncertainty associated with the laser spectral purity. The negligible difference obtained between the K_a values by the two independent techniques at 10.60358 μm (both 239 cm^{-1}) would suggest an accuracy of 1 cm^{-1}, but this result was obtained after averaging over many samples. Sample-to-sample variations (see Fig. 6) indicate a larger uncertainty interval of ±15 cm^{-1} for 20:1 confidence.

Summary

Quantitative determination of the infrared optical constants of AP and HTPB binder (2.5–18 μm) was performed using FTIR spectroscopic transmission measurements. Spectral subtraction and baseline shifting methods were applied to the FTIR AP/KBr pellet data to account for KBr matrix scattering. An independent spectral subtraction technique was developed based on laser spatial filtering to verify the FTIR results. In both KBr pellet techniques (FTIR and laser) the Rayleigh–Gans limit of scattering was exploited to establish a relationship between the apparent pellet absorption properties and the intrinsic AP absorption coefficient. Dispersion theory was used to determine refractive index from absorption index for AP.

Acknowledgments

Support for this work from the Office of Naval Research, N00014-91-J-1977, is gratefully acknowledged. Richard S. Miller was the Scientific Officer. We are also indebted to Richard O. Buckius and Jeff Ford of the University of Illinois for use of the FTIR spectrometer.

References

[1]Griffiths, P. R., and De Hasath, J. A., *Fourier Transform Infrared Spectrometry*, Wiley, New York, 1986.
[2]Bohren, C. F., and Huffman, D. R., *Absorption and Scattering of Light by Small Particles*, Wiley, New York, 1983.
[3]Sahba, N., and Rockett, T. J., "Infrared Absorption Coefficients of Silica Glasses," *Journal of American Ceramic Society*, Vol. 75, No. 1, 1992, pp. 209–212.
[4]Brewster, M. Q., and Kunitomo, T., "The Optical Constants of Coal, Char, and Limestone," *Journal of Heat Transfer*, Vol. 106, 1984, pp. 678–683.
[5]Grosse, P., and Offermann, V., "Analysis of Reflectance Data Using the Kramers-Kronig Relations," *Applied Physics A*, Vol. 52, 1991, pp. 138–144.
[6]Vartiainen, E. M., Peiponen, K.-E., and Asakura, T., "Comparison Between the Optical Constants Obtained by Kramers-Kronig Analysis and the Maximum Entropy Method: Infrared Optical Properties of Orthorhombic Sulfur," *Applied Optics*, Vol. 32, No. 7, 1993, pp. 1126–1129.
[7]Verleur, H. W., "Determination of Optical Constants from Reflectance or Transmittance Measurements on Bulk Crystals or Thin Films," *Journal of the Optical Society of America*, Vol. 58, No. 10, 1968, pp. 1356–1364.
[8]Patel, R. S., and Brewster, M. Q., "Optical Constants of Propellant-Grade Ammonium Perchlorate," *AIAA Journal*, Vol. 24, No. 11, 1986, pp. 1878–1880.
[9]Brewster, M. Q., *Thermal Radiative Transfer and Properties*, Wiley, New York, 1992.
[10]Isbell, R. A., "Optical Properties of Energetic Materials: AP, RDX, HMX, HTPB Binder, and N5," M.S. Thesis, Univ. of Illinois, Urbana, IL, 1995.
[11]Ross, S. D., "Forbidden Transitions in the Infra-Red Spectra of some Tetrahedral Anions — I. Perchlorates," *Spectrochimica Acta*, Vol. 18, 1962, pp. 225–228.
[12]Waddington, T. C., "Infrared Spectra, Structure, and Hydrogen-Bonding in Ammonium Salts," *Journal of the Chemical Society*, Pt. IV, 1958, pp. 4340–4344.
[13]Petricciani, J. C., Wiberley, S. E., Bauer, W. H., and Clapper, T. W., "The Effects of a Chlorate Impurity on the Thermal Stability of Ammonium Perchlorate," *Journal of Physical Chemistry*, Vol. 64, 1960, pp. 1309–1311.
[14]Herzberg, G., *Infra-Red and Raman Spectra of Polyatomic Molecules*, Van Nostrand, New York, 1945, p. 167.
[15]Carter, J. C., and Devia, J. E., "Vibrational Analysis of Methylcarbamate and N,N-Dichloromethylcarbamate," *Spectrochimica Acta*, Vol. 29A, 1973, pp. 623–632.
[16]Chen, J. K., Cheng, S. S., and Chou, S. C., "DSC, TG and Infrared Spectroscopic Studies of HTPB and Butacene Propellant Polymers," AIAA Paper 94-3176, 1994.
[17]Nyquist, R. A., "Infrared Spectra-Structure Correlations of Carbamic Acid: Aryl-, Alkyl Esters," *Spectrochimica Acta*, Vol. 29A, 1973, pp. 1635–1641.